Lyotropic Mesophase Formation of Imogolite (Commemoration Issue Dedicated to Professor Hiroshi Ibagaki, Professor Michio Kurata, Professor Ryozo Kitamura, On the Occasion of Their Retirments)

AUTHOR(S):

Kajiwara, Kanji; Urakawa, Hiroshi; Donkai, Nobuo; Hiragi, Yuzuru; Inagaki, Hiroshi; Schmidt, Manfred

CITATION:

Kajiwara, Kanji ...[et al]. Lyotropic Mesophase Formation of Imogolite (Commemoration Issue Dedicated to Professor Hiroshi Ibagaki, Professor Michio Kurata, Professor Ryozo Kitamura, On the Occasion of Their Retirments). Bulletin of the Institute for Chemical Research, Kyoto University 1989, 66(3): 165-175

ISSUE DATE:

1989-02-15

URL:

http://hdl.handle.net/2433/77245

Bull. Inst. Chem. Res., Kyoto Univ., Vol. 66, No. 3, 1988

Lyotropic Mesophase Formation of Imogolite

Kanji KAJIWARA*, Hiroshi URAKAWA*, Nobuo DONKAI**,
Yuzuru HIRAGI**, Hiroshi INAGAKI**,
Manfred SCHMIDT***

Received August 24, 1988

The process of mesophase formation was observed in the aqueous solutions of natural polymer, imogolite, by means of small-angle X-ray scattering. Scattered intensities from the imogolite solutions were Fourier-transformed to yield the distance distribution function in real space. The results, together with the results of polarized and depolarized light scatterings, indicate that the imogolite molecules assemble side by side with their ends being rather arranged at the initial stage of agregation, and form loosely packed pencil-shaped units. These pencil-shaped units eventually assemble in raft-like sheets to form mesophase above the A-point where the ridges corresponding to the edges of pencil-shaped units run parallely with an interval of 175Å on the surface of the formed sheet. This process of mesophase formation was demonstrated schematically by assembling and arranging imogolite repeat units.

KEY WORDS: Imogolite/ Lyotropic mesophase/ Light scattering/ Small-angle X-ray scattering/ Optical anisotropy

INTRODUCTION

Imogolite, a natural product found first in the clay fraction of Japanese soil derived from glassy volcanic ash or in weathered pumice beds, is a cylinder-shaped inorganic polymer composed of hydrated alumina silicates. Imogolite is molecularly dispersed in acidic aqueous solution of pH$<$3 where most of the Al(OH)-groups are protonated, and is completely rigid in solution as proved by viscometry and dynamic/static light scattering.[1] For example, the intrinsic viscosity $[\eta]$ of a rigid rod is expected to be approximately in proportion to the square of the molecular weight as given by

$$[\eta] \sim L_w^2/\ln (L_w/d) \tag{1}$$

and the hydrodynamic radius R_H to the molecluar weight as given by

$$R_H \sim L_w/[\ln (L_w/d)] \tag{2}$$

when the rod length is sufficiently large. Here the weight-average rod length of imogolite L_w is evaluated from the weight-average molecular weight M_w as

$$L_w \sim 8.4 \times (M_w/4754) \quad (\text{Å}) \tag{3}$$

with 8.4 Å and 4754 being the length and the molecular weight of an imogolite repeat

* 梶原莞爾，浦川　宏：Faculty of Engineering and Design, Kyoto Institute of Technology, Kyoto, Sakyo-ku, Matsugasaki, 606
** 呑海信雄，柊　弓弦，稲垣　博：Institute for Chemical Research, Kyoto University, Kyoto-fu, Uji, 611
*** MPI fur Polymerforschung, Postfach 3148, 6500 Mainz, BRD.

unit, respectively. Here d denotes a hydrodynamically effective diameter which is in practice equivalent to the cylinder diameter of imogolite. The radius of gyration of a rigid rod is given as

$$\langle s^2 \rangle_z^{1/2} = L_w/12 \tag{4}$$

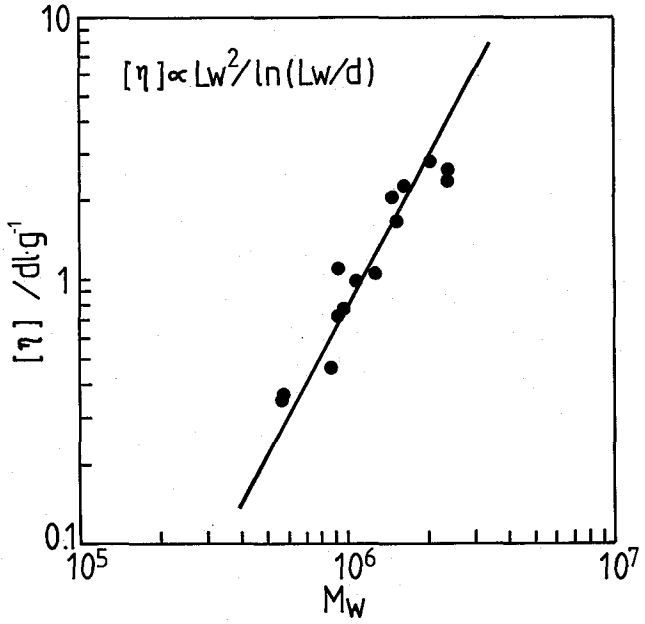

Figure 1. Intrinsic viscosity of imogolite as a function of molecular weight. A solid line in the figure represents the relation specified by eq. (1).

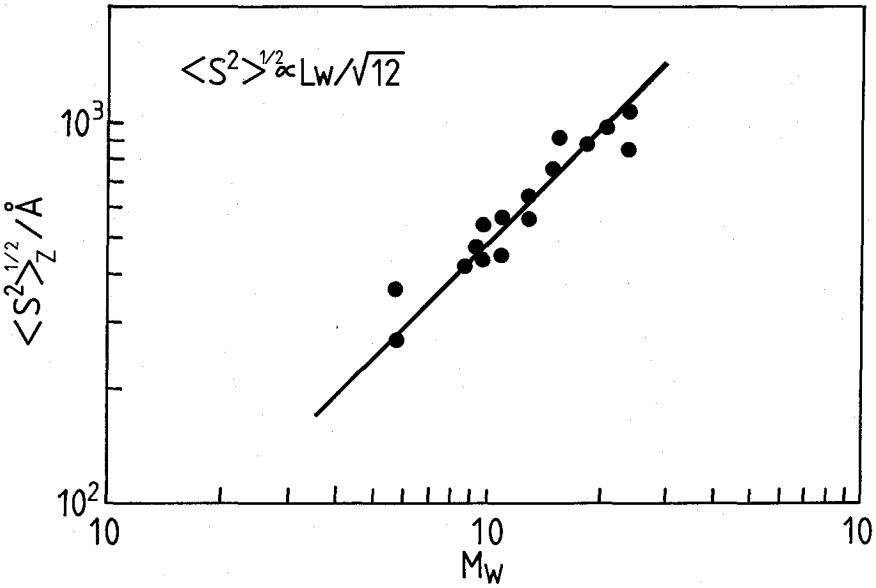

Figure 2. Radius of gyration of imogolite as a function of molecular weight. A solid line in the figure represents the relation specified by eq. (4).

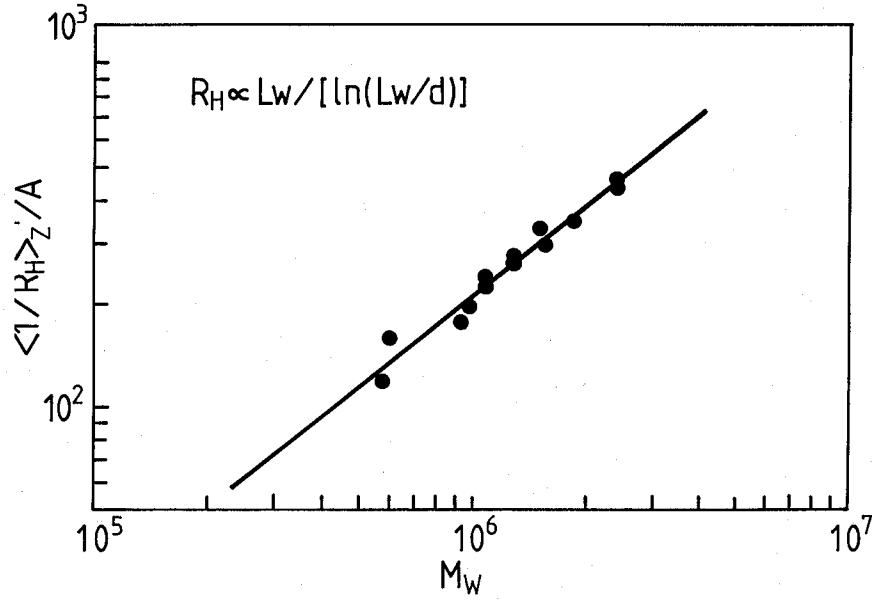

Figure 3. Hydrodynamic radius of imogolite as a function of molecular weight. A solid line in the figure represents the relation specified by eq. (2).

These expected relations for a rigid rod (eqs. (1), (2) and (4)) are observed experimentally as shown in Figs. 1–3, proving a totally rigid structure of an imogolite cylinder. As expected from its shape, imogolite forms lyotropic mesophase when the imogolite concentration exceeds a certain limiting point defined as an A-point[2]. The imogolite mesophase was observed electron-microscopically as a raft-like sheet exhibiting various periodic structures[3]. The mesophase also exhibits the cholesteric characteristics when observed through a polarizing microscope. Here the cholesteric pitch was found to depend on the solute concentration in an inverse manner but not on the molecular weight (i.e., the rod length). No account was so far found for the origin of the cholesteric order of the imogolite mesophase. In the present report, we observe the process of the mesophase formation of imogolite by means of small-angle X-ray scattering (SAXS). The preliminary results of polarized and depolarized light scattering will be introduced to suffice the conclusion drawn from the SAXS results.

EXPERIMENTAL PART

Sample Preparation

Imogolite solutions of various concentrations were prepared according to the procedure described previously[1]. Those solutions were dialyzed against a sufficient amount of aqueous solution containing 1.20 vol.% acetic acid and 0.02 wt.% NaN_3 for 5 to 7 days in cellulose tubes (Visking Co., Chicago, U.S.A.). Each dialyzed solution was filtered through ultracellafilter membranes Type SM (Sartorius Co., W. Germany) in prior to scattering experiments. A concentration of each solution was determined from

the refractive index difference between the solution and the dialyzate.

Two fractionated imogolite samples were employed where the characteristics of these samples are summarized in Table 1. The figures in the brackets in Table 1 denote respective rod lengths (in Å) of Imogolites a and e, calculated from the molecular weights, the radii of gyration and the hydrodynamic radii, using eqs. (2), (3) and (4). Considering the consistency of estimated rod lengths from both radii (the radius of gyration and the hydrodynamic radius), the molecular weights seem to be overestimated probably due to a large error involoved in evaluating the refractive index increment. The A-point and B-point of the mesophase (lower and upper phase boundary concentrations) were estimated as 0.0355 and 0.0577 for Imogolite a, and as 0.0175 and 0.0333 for Imogolite e, respectively, in terms of imogolite weight fraction.

Table 1. Characteristics of Imogolite Samples

Imogolite	$M_w \times 10^{-6}$	$\langle S_2 \rangle_z^{1/2}$ (Å)	R_H (Å)
a	0.980 (1732Å)	438 (1517Å)	180 (1462Å)
e	2.43 (4294Å)	1053 (3647Å)	386 (3890Å)

Figures in brackets denote the rod length estimated form respective observed quantitites, using eqs. (2), (3) and (4).

Light Scattering

Polarized and depolarized, dynamic and static light scatterings from imogolite solutions (the concentration varies from 0.5 g/l to 21.5 g/l) were simultaneously measured with an ALV photon correlator system equipped with an argon ion laser (λ_0=488 nm).

The polarized and depolarized static light scattering intensities from optically anisotropic molecules yield apparent quantities when evaluated according to Zimm's procedure. These quantities are related with the true values as[4]

$$(M_w^{app})^{VV} = M_w(5+4\delta^2)/5 \tag{5}$$

$$(\langle S^2 \rangle_z^{app})^{VV} = \langle S^2 \rangle_z (1-4/5\delta+4/7\delta^2)/(1+4/5\delta^2) \tag{6}$$

for polarized components, and

$$(M_w^{app})^{VH} = M_w(3\delta^2/5) \tag{7}$$

$$(\langle S^2 \rangle_z^{app})^{VH} = 9\langle S^2 \rangle_z/7 \tag{8}$$

for depolarized components. Here δ denotes the overall chain anisotropy which is equivalent to the intrinsic anisotropy factor δ_0 defined by

$$\delta_0 = (\alpha_{//} - \alpha_\perp) / (\alpha_{//} + 2\alpha_\perp) \tag{9}$$

with $\alpha_{//}$ and $\alpha_\perp$ being the polarizabilities parallel and perpendicular to the chain axis, respectively, in the case of a rigid cylinder. δ_0 should lie in the range of $-1/2 < \delta_0 < 1$ as seen from eq. (9).

The first cumulant Γ is determined by a cumulant fit of the normalized logarithmic correlation function observed in the dynamic scatteing experiments, and is given at small q in the polarized experiments by

$$\Gamma/q^2=D_z(1+C\langle S^2\rangle_z q^2+\cdots) \tag{10}$$

with D_z and C being the z-average diffusion coefficient and a quantity which depends on the molecular structure, respectively. Here Γ approaches to zero as $q\rightarrow 0$. The rotational diffusion coefficient θ is measured in the limit of $q\rightarrow 0$ in the case of the depolarized dynamic scattering as[6]

$$\lim \Gamma=6\theta \tag{11}$$

The rotational diffusion coefficient θ is calculated for an ellipsoid of revolution with major semiaxis a and minor semiaxis b by Perrin[7] as

$$\theta=(3kT/16\pi\eta\, a^3)[\{(2-p)G(p)-1\}/(1-p^2)] \tag{12}$$

where p denotes the axial ratio (p=b/a), η the shear viscosity of the solution and G(p) a function of the axial ratio given by

$$G(p)=(1-p^2)^{-1/2}\ \ln\ [\{1+(1-p^2)^{1/2}\}/p] \tag{13}$$

for prolate ellipsoid, $p<1$. The translational diffusion coefficient D is given for this ellipsoid model in terms of the function G(p) as

$$D=kTG(p)/6\pi\eta\, a \tag{14}$$

which yields eq. (2) in the limit of $p<<1$.

Small-Angle X-Ray Scattaring

The small-angle X-ray scattering (SAXS) measurements were performed with a SAXES focusing optics installed at the BC-10C of the Photon Factory, Tsukuba, Japan[8]. The scattered intensity I(q) was Fourier-transformed to the distance distribution function defined as:

$$p(r)=(2\pi)^{-1}\int_0^\infty I(q)\cdot(qr)\cdot\sin(qr)\ dq \tag{15}$$

Here the scattered intensity was extrapolated to both zero and larger angles according to the second-order polynomial approximation and Porod's 4-th power law[9], respectively, in order to minimize the cut-off effect.

RESULTS AND DISCUSSION

Fig. 4 demonstrates the concentration dependence of the scattered polarized and depolarized light intensities in the limit of $q\rightarrow 0$ for Imogolite a. A drop of the apparent scattered intensities at higher concentrations indicates the onset of aggregation. The molecular anisotropy was estimated as $\delta=0.135$ for Imogolite a and $\delta=0.128$ for Imogolite e from the ratio of the polarized and depolarized apparent molecular weights:

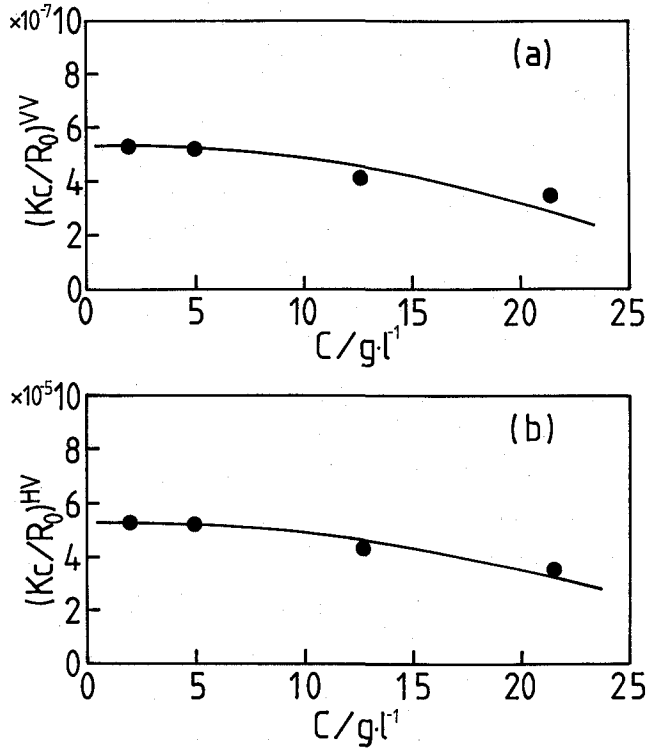

Figure 4. Polarized (a) and depolarized (b) scattered light intensities at q→0 as a function of imogolite concentration (Imogolite a).

$$(M_w^{app})^{VV}/(M_w^{app})^{VH}=(5+4\delta^2)/(3\delta^2) \tag{16}$$

These values are rather small in comparison with those so far reported for a rigid-rod type moelcule, indicating a rather small difference between polarizabilities porallel and perpendicular to the chain axis. For example, $\delta=0.3$ for tabacco mosaic virus, and $\delta=0.38$ for heterocyclic ladder polymer are estimated. The angular dependence of polarized and depolarized scattering light intensities exhibits a marked difference in its behavior. The polarized scattering light intensities decreases monotoneously with increasing the scattered angle as expected, while the depolarized scattering light intensities show a miximum in the zimm plot (see Fig. 5). This maximum is much pronounced and located at smaller q than that calculated by Horn[4]. Since neither the position of this maximum nor its relative intensity with respect to the extrapolated intersity to $q=0$ varies with the concentration or molecular weight of imogolite, this maximum seems to be caused by an intramolecular structure.

Fig. 6 shows the polarized and depolarized first cumulant Γ/q^2 as a function of q^2 for Imogolite a where the strong concentration dependence of the apparent diffusion coefficient Γ^{VV}/q^2 indicates the aggregation of imogolite molecules in higher concentrations. The apparent translational diffusion coefficients are summarized in Table 2 as

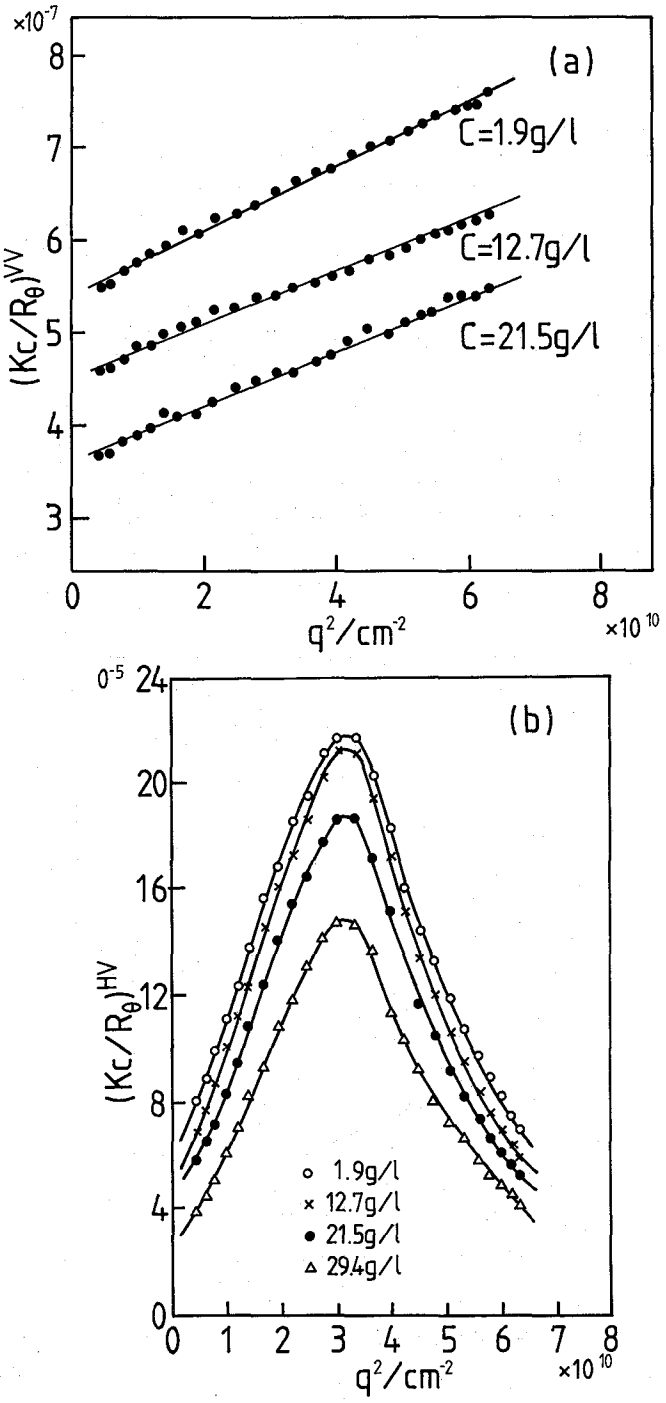

Figure 5. Zimm plot of polarized (a) and depolarized (b) scattered light intensities (Imogolite a).

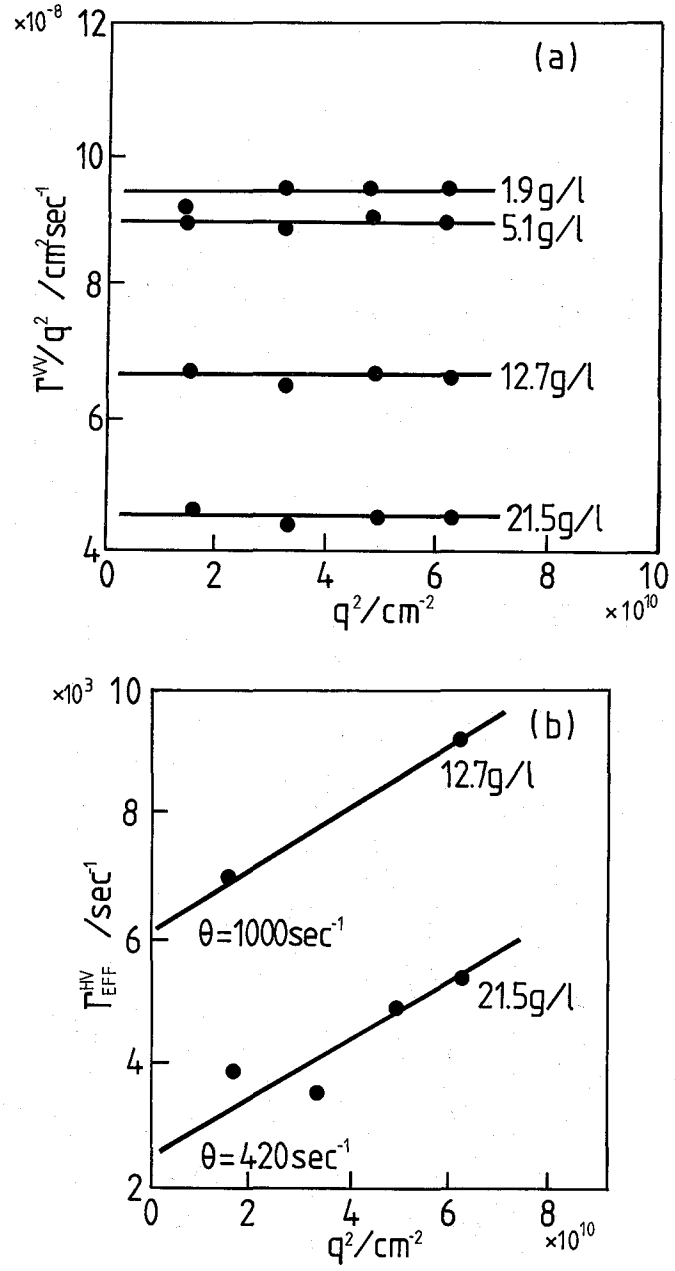

Figure 6. Polarized (a) and depolarized (b) first cumulant as a function of q^2 (Imogoliote a).

estimated from the polarized first cumulants. The measured depolarized first cumulant yields the "true" cumulant by multiplying the measured static depolarized structure factor as

$$\Gamma^{HV}{}_{EFF} = \Gamma^{HV} \cdot S^{HV}(q) \tag{17}$$

Table 2. Apparent Translational (D_z) and Rotational Diffusion (θ) Cofficient as a Function of Imogolite Concentration

c (g/l)	D_z ($cm^2 \cdot sec^{-1}$)	θ (sec^{-1})
1.98	9.45×10^{-8}	
5.10	9.20×10^{-8}	
12.7	6.68×10^{-8}	1000
21.5	4.78×10^{-8}	420

where Γ^{HV}_{EFF} and $S^{HV}(q)$ denote the depolarized "true" first cumulant and the measured depolarized structure factor. Though no reliable extrapolation can be made, Γ^{HV}_{EFF} in the limit of $q\to0$ estimates the rotational diffusion coefficient from eq. (11) as $\theta=1000\ sec^{-1}$ and $\theta=420\ sec^{-1}$ for Imogolite a at the concentrations 12.7 g/l and 21.5 g/l, respectively. The ratio of the rotational to the translational diffusion coefficient yields from eqs. (12) and (14):

$$\theta/D=(9/8a^2)(2-G(p)^{-1}) \tag{18}$$

when $p<<1$ where G(p) is approximated as

$$G(p)\simeq \ln(2L_w/d). \tag{19}$$

Since $\ln(2L_w/d)$ varies only from 5.3 to 7.6 with L_w/d varying from 100 to 1000, the factor $(2-G(p)^{-1})$ is nearly constant, varying from 1.81 to 1.87 accordingly, and the ratio is given as

$$\theta/D=A/L_w^2 \tag{20}$$

where $A=2.04$ or 2.10 for $L_w/d=100$ or 1000, respectively. Assuming A is constant and equal to 2.10, the rod length L_w is evaluated from the ratio of the rotational to the translational diffusion coefficient as 1184 Å or 1546 Å, respectively, at c=12.7 g/l or 21.5 g/l. As seen from Table 1, the rod length evaluated from the ratio eq. (20) is close to an intrinsic rod length of Imogolite a, though a large error might be involved in estimating a rotational diffusion coefficient. This result suggests that the imogolite molecules are arranged side by side with their ends rather in order at the initial stage of aggregation.

The distance distribution function (see eq. (15)) of the imogolite mesophase is marked by the double peaks around 25 to 50 Å and 175 Å which appears when the imogolite concentration exceeds the A-point. Below the A-point, the distance distribution function has a shoulder around 30 Å which corresponds the cross-section of a single imogolite molecule, and a broad peak around 75 Å. A further peak appears around 270 Å when the imogolite concentration approaches to the B-point as shown in Fig. 7. When left the solution above the B-point for days, the solution forms gel which is apparently thixotropic. The structure of this gel is not known except cholesteric swirls exhibited by the gel under the polarizing microscope. Considering the various periodic structure observed by the electron microscope, imogolite molecules gradually

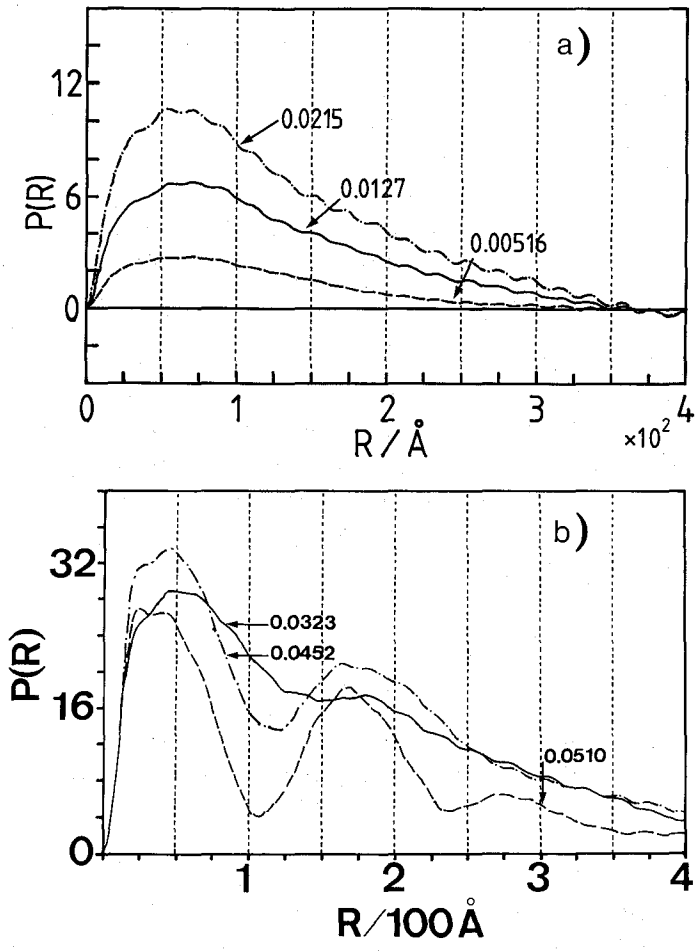

Figure 7. Distance distribution functions of Imogolite a solutions of various concentrations. (a) Below the A-point. (b) Above the A-Point.

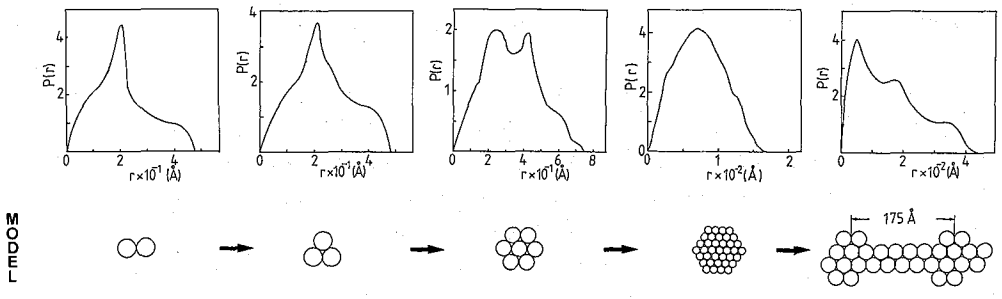

Figure 8. Schematic model of imogolite aggregates and computed distance distribution functions. Each circle in the schematic models denotes a single imogolite repeat unit of 8.4 Å in length and 25 Å in diameter.

assemble together in loosely packed pencil-like (hexagonal) shapes of the length of a single imogolite molecule, and these pencil-shaped unite will be arranged by side to side in raft-like sheet to form mesophase above the A-point. Here the peak will appear around 175 Å, suggesting the ridges run parallely with an interval of 175 Å on the surface of the formed sheet. These ridges correspond to the edges of pencil-shaped imogolite assemblies formed in prior to the A-point. Since the pencil-shaped units are formed and re-specify the volume fraction, the A-point will shift to a lower concentration than that predicted by Onsager. This process of forming pencil-shaped units and raft-like sheets are demonstrated schematically by assembling and arranging imogolite repeat units as shown in Fig. 8. These ensembles of imogolite repeat units yield the distance distribution functions similar to those observed in due course of mesophase formation.

ACKNOWLEDGEMENT

The small-angle X-ray scattering measurements were performed at Photon Factory, Tsukuba, under the project scheme of the proposal No. 86–060 as approved by the Photon Factory Advisory Committee which is thus acknowledged. K.K. is indebted to the AvH-Stiftung and the SFB 60 for a grant, and N.D. acknowleges the MPI for a financial support to a part of this work.

REFERENCES

1) N. Donkai, H. Inagaki, K. Kajiwara, H. Urakawa, M. Schmidt, *Makromol. Chem.*, **186**, 2623 (1985).
2) K. Kajiwara, N. Donkai, Y. Hiragi, H. Inagaki, *Makromol. Chem.*, **187**, 2883 (1986).
3) K. Kajiwara, N. Donkai, Y. Fujiyoshi, H. Inagaki, *Makromol. Chem.*, **187**, 2895 (1986).
4) P. Horn, *Ann. de Phys.*, **10**, 386 (1956).
5) See, for example, W. Burchard, *Adv. Polym. Sci.*, **48**, 1 (1983).
6) B. J. Berne, R. Pecora, "*Dynamic Light Scattering*", John Wiley, New York, 1976.
7) F. Perrin, *J. de Phys. et Rad.*, **5**, 497 (1934); **7**, 1 (1936).
8) T. Ueki, Y. Hiragi, Y. Izumi, H. Tagawa, M. Kataoka, Y. Muroga, T. Matsushita, Y. Amemiya, *Photon Factory Report*, **VI70, (1983).**
9) G. Porod, in "*Small Angle X-ray Scattering*" (ed. by O. Glatter and O. Kratky), Academic Press, London, 1982.